Nano Research 2018, 11(12): 6167–6176
https://doi.org/10.1007/s12274-018-2133-6
Research Article
ISSN 1998-0124
CN 11-5974/O4

Background-free latent fingerprint imaging based on nanocrystals with long-lived luminescence and pH-guided recognition

Zhiheng Li[1,§], Qian Wang[1,§], Yingqian Wang[1,§], Qinqin Ma[1], Jie Wang[1], Zhihao Li[1], Yingxue Li[1], Xiaobo Lv[1], Wei Wei[2], Lang Chen[3], and Quan Yuan[1] (✉)

[1] *Key Laboratory of Analytical Chemistry for Biology and Medicine (Ministry of Education), College of Chemistry and Molecular Sciences, Wuhan University, Wuhan 430072, China*
[2] *State Key Laboratory of Biochemical Engineering, Institute of Process Engineering, Chinese Academy of Sciences, Beijing 10090, China*
[3] *School of Basic Medical Sciences, Wuhan University, Wuhan 430072, China*
[§] *Zhiheng Li, Qian Wang and Yingqian Wang contributed equally to this work.*

Received: 1 May 2018
Revised: 8 June 2018
Accepted: 13 June 2018

KEYWORDS
fingerprint,
persistent luminescence,
background interference,
nanoparticle,
imaging

ABSTRACT

Latent fingerprints (LFPs) are highly specific to individuals, and LFP imaging has played an important role in areas such as forensic investigation and law enforcement. Presently, LFP imaging still faces considerable problems, including background interference and destructive and complex operations. Herein, we have designed a background-free, nondestructive, and easy-to-perform method for LFP imaging based on pH-mediated recognition of LFPs by carboxyl group-functionalized Zn_2GeO_4:Mn (ZGO:Mn-COOH) persistent luminescence nanorods (PLNRs). By simply adjusting the pH of the ZGO:Mn-COOH colloid dispersion to a certain acidic range, the negatively charged ZGO:Mn-COOH readily binds to protonated fingerprint ridges via electrostatic attraction. The ZGO:Mn-COOH colloid dispersion can be stored in portable commercial spray bottles, and the LFPs have been easily detected *in situ* by simply dropping the colloid dispersion on the LFPs. Moreover, since the ZGO:Mn-COOH can remain luminescent after excitation ceases, background color and background fluorescence interference were efficiently removed by simply capturing the luminescent LFP images after the excitation ceased. The entire LFP imaging process can be easily conducted without any destructive or complex operations. Due to the great versatility of the developed method for LFP imaging, clear LFP images with well-resolved ridge patterns were obtained. The designed background-free, nondestructive, and easy-to-perform LFP imaging strategy has great potential for future applications, such as forensic investigations and law enforcement.

Address correspondence to yuanquan@whu.edu.cn

1 Introduction

Since no two individuals possess identical finger patterns, fingerprints have long been utilized as one of the most useful forms of proof for personal identification and have been widely used in areas such as forensic investigation, law enforcement, and access control [1–6]. Most fingerprints are invisible to the naked eye and are called latent fingerprints (LFPs) [7–10]. In the past decades, a variety of optical contrast agents have been developed for LFP imaging [11–15], such as nanoparticles with absorption or emission in the visible region [16–19]. Even though great advances have been made in LFP imaging [20], there are still several problems that need to be overcome. LFP imaging usually suffers from background signal interference, since the underlying substrates contain compounds that possess optical properties similar to that of the contrast agents [9, 19, 21, 22]. Background interference, such as background color and background fluorescence, usually makes the LFP images blurred and drastically decreases the imaging sensitivity and resolution [19, 22]. Moreover, in LFP imaging, the contrast agents should be attached to LFP ridges by a nondestructive and simple method. Previous studies suggest that methods such as powder dusting cause inevitable destruction to fingerprint details, leading to loss of the detailed ridge pattern and chemical information [23]. Therefore, it is important to develop a background-free, nondestructive, and easy-to-perform method for LFP imaging.

Persistent phosphors possess the special ability to remain luminescent after excitation ceases [24–28]. Since background fluorescence disappears rapidly after the excitation ceases [29–32], persistent phosphors can efficiently avoid background fluorescence interference by collecting the persistent luminescence signal after the background fluorescence has decayed completely [33–39]. Moreover, since the color of the substrates bearing the LFPs is invisible after excitation ceases, persistent phosphors can also eliminate background color interference in LFP imaging. Therefore, persistent phosphors are ideal candidates for developing background-free methods for LFP imaging.

Previous studies reported that proteins and amino acids in fingerprints are protonated to carry a positive charge in acidic conditions [40]. Thus, contrast agents that carry a negative charge in acidic conditions can readily bind to fingerprint ridges via electrostatic attraction [40–42]. Also, hydrophobic interactions are believed to contribute to the binding of negatively charged contrast agents to the positively charged fingerprints [41]. In LFP detection based on electrostatic interactions, fingerprint details can be well-retained since no external operations such as brushing are involved, reflecting the non-destructive nature of this method. Moreover, the binding of contrast agents to fingerprint ridges can be easily achieved by simply applying a solution with a low pH value [42]. Thus, electrostatic interactions are used to develop nondestructive and easy-to-perform methods for LFP imaging.

Herein, we report a background-free, nondestructive, and easy-to-perform method for LFP imaging based on carboxyl group-functionalized Zn_2GeO_4:Mn (ZGO:Mn-COOH) persistent luminescence nanorods (PLNRs) with a pH-driven electrostatic recognition function. As shown in Scheme 1, the acidic ZGO:Mn-COOH colloid dispersion, stored in a portable spray bottle, is dropped onto the LFPs. Within a certain acidic pH range, the ZGO:Mn PLNRs are still negatively charged, whereas the proteins and amino acids in the LFPs are protonated to be positively charged. As a result, the ZGO:Mn PLNRs specifically bind to LFP ridges via electrostatic interactions. Under excitation,

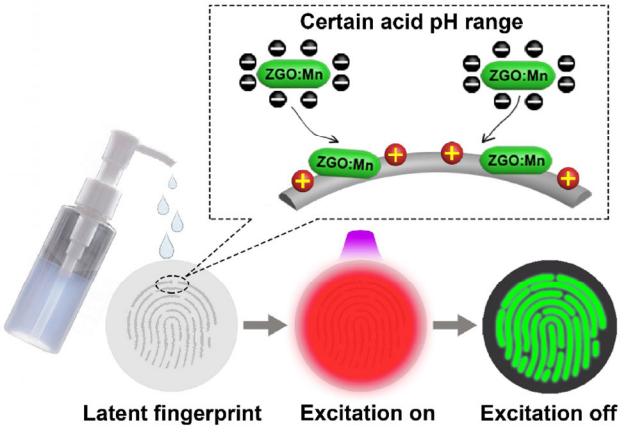

Scheme 1 Schematic illustration of the background-free, nondestructive, and easy-to-perform LFP imaging method with the ZGO:Mn-COOH PLNRs. The ZGO:Mn-COOH PLNRs bind to fingerprint ridges via electrostatic attraction within a certain acidic pH range.

background signals such as background fluorescence and background color appear, causing the image of the LFPs to be significantly blurred. After excitation ceases, the background signals disappear rapidly, whereas the ZGO:Mn PLNRs remain luminescent and show a clear fingerprint image. In this strategy, no destructive operations are involved, and the ZGO:Mn PLNRs can specifically bind to the LFPs with only an adjustment of the pH of the ZGO:Mn colloid dispersion. Moreover, interference from background fluorescence or background color is efficiently eliminated by the ZGO:Mn PLNRs. Thus, this pH-mediated LFP imaging strategy is background-free, nondestructive, and easy-to-perform, making it valuable in fields such as forensic investigation and law enforcement.

2 Experimental

2.1 Synthesis of the Zn_2GeO_4:0.5%Mn (ZGO:Mn) PLNRs

The ZGO:Mn PLNRs were synthesized by a modified hydrothermal method [25, 33]. Typically, 11 mL of reaction solution containing 2 mmol of $Zn(NO_3)_2$, 0.005 mmol of $Mn(NO_3)_2$, and 300 μL of concentrated HNO_3 was prepared. Then, 1 mmol of Na_2GeO_3 was added dropwise to the above reaction solution under vigorous stirring. The pH of the resultant solution was adjusted to 9.5 with ammonium hydroxide (28 wt.%). Then, the reaction mixture was transferred into a Teflon-lined autoclave and allowed to react at 220 ℃ for 12 h. The resulting ZGO:Mn PLNRs were further collected by centrifugation and washed three times with deionized water.

2.2 Preparation of the ZGO:Mn-COOH PLNRs

Firstly, the ZGO:Mn PLNPs were modified with amino groups (ZGO:Mn-NH_2) through the hydrolysis of (3-aminopropyl) triethoxysilane (APTES) on their surface. Typically, 100 mg of ZGO:Mn PLNPs were dispersed in 40 mL of dimethylformamide (DMF) under sonication. After, 400 μL of APTES was slowly added into the DMF dispersion under vigorous stirring. The resultant solution was allowed to react at 80 ℃ for 12 h under vigorous stirring. Then, the resultant ZGO:Mn-NH_2 PLNRs were collected by centrifugation and washed three times with DMF.

Next, the ZGO:Mn-COOH PLNPs were prepared through the reaction of ZGO:Mn-NH_2 with succinic anhydride. Briefly, the obtained ZGO:Mn-NH_2 PLNRs were dispersed in 40 mL of DMF. After, 20 mL of succinic anhydride solution (5 mg/mL in DMF) and 20 mL of DMAP solution (0.5 mg/mL in DMF) was slowly added to the ZGO:Mn-NH_2 colloid dispersion. The resultant reaction solution was allowed to react at room temperature for 12 h under vigorous stirring. The as prepared ZGO:Mn-COOH PLNRs were also collected by centrifugation and washed with ethanol/water (v/v, 1:1) three times.

2.3 Collection of LFPs

The fingerprint donors were asked not to wash their hands 1 h prior to the collection. The LFPs were collected by the donors pressing their fingers on the chosen substrates. After, a hydrophobic circle was drawn around each fingerprint to keep the ZGO:Mn-COOH PLNR colloid dispersion over the fingerprints. In this study, aluminum foil, a glass slide, a soda can, cardboard, a mobile phone display screen, a wineglass, scissors, a silicon slice, and wood were used as the substrates to deposit the LFPs. During pH optimization, the LFPs were deposited on aluminum foil. For the confocal microscopy measurement, the LFPs were deposited on glass slides. While imaging the LFPs from different donors, the LFPs were also deposited on aluminum foil.

2.4 The pH optimization for LFPs imaging

ZGO:Mn-COOH PLNR colloid dispersions (0.5 mg/mL) with pH values ranging from 3 to 5 were systematically prepared with HCl and transferred to commercial spray bottles. Typically, the colloid dispersions were added dropwise to the LFPs with the spray bottle until the LFPs were covered. After reacting for about 30 min, the LFPs were rinsed with water to remove the unbound ZGO:Mn-COOH PLNRs remaining on the substrate. The fingerprint images were captured with a digital single-lens reflex camera under ultraviolet (UV) excitation.

2.5 Confocal microscopy measurements

To visualize the LFP ridges using confocal microscopy, the LFPs were labeled with a hydrophobic red dye, DiD. The labeling of LFPs was conducted as follows. Typically, a small volume of DiD solution (10 μL, 5 nM) was spread on the fingertips of donors. After drying, the donors pressed their fingers on glass slides to prepare the labeled LFPs. For LFP imaging, a ZGO:Mn-COOH PLNR colloid dispersion with a pH of 3.5 was used. For the confocal microscopy measurements, a 405 nm laser was used to activate the ZGO:Mn-COOH PLNRs attached to the LFPs.

2.6 Background-free LFP imaging with the ZGO:Mn-COOH PLNRs

The LFPs on the soda can and cardboard were treated with a ZGO:Mn-COOH PLNR colloid dispersion at pH of 3.5. After the reaction, the developed LFPs were illuminated with a portable UV lamp to activate the ZGO:Mn-COOH PLNRs. Videos of the LFPs were taken upon ceasing the UV excitation to record the decay of the luminescent images. The videos were played with the PotPlayer software (Daum, 1.6.60136.0) to find frames in which background fluorescence had decayed completely but the ZGO:Mn-COOH PLNRs remained luminescent. In the LFP imaging method with the optical filtering, a 510 nm long-pass filter was employed to block the passage of blue background fluorescence from the cardboard.

3 Results and discussion

3.1 Characterization of the carboxyl group-modified ZGO:Mn PLNRs

The ZGO:Mn PLNRs were synthesized using a modified hydrothermal method [25, 33]. The prepared ZGO:Mn PLNRs were functionalized with amino groups through the hydrolysis of APTES on their surface (Fig. 1(a)), then the nanorods were further reacted with succinic anhydride to obtain ZGO:Mn-COOH PLNRs. The shape and size of the ZGO:Mn-COOH PLNRs were characterized with transmission electron microscopy (TEM). As shown in Fig. 1(b), the ZGO:Mn-COOH PLNRs were well dispersed with a typical rod shape. Energy-dispersive X-ray (EDX) analysis (Fig. 1(c)) confirmed the successful doping of Mn in the ZGO:Mn-COOH PLNRs. The luminescence properties of the ZGO:Mn-COOH were further investigated. As shown in Fig. 1(d), the emission band of ZGO:Mn-COOH peaked at around 534 nm, which is attributed to the $^4T_1(G)$–$^6A_1(S)$ transition of Mn^{2+} [25]. The inset in Fig. 1(d) indicates that the ZGO:Mn-COOH PLNRs were well-dispersed in the aqueous solution, and the colloid dispersion showed strong green emission under excitation. The ZGO:Mn-COOH

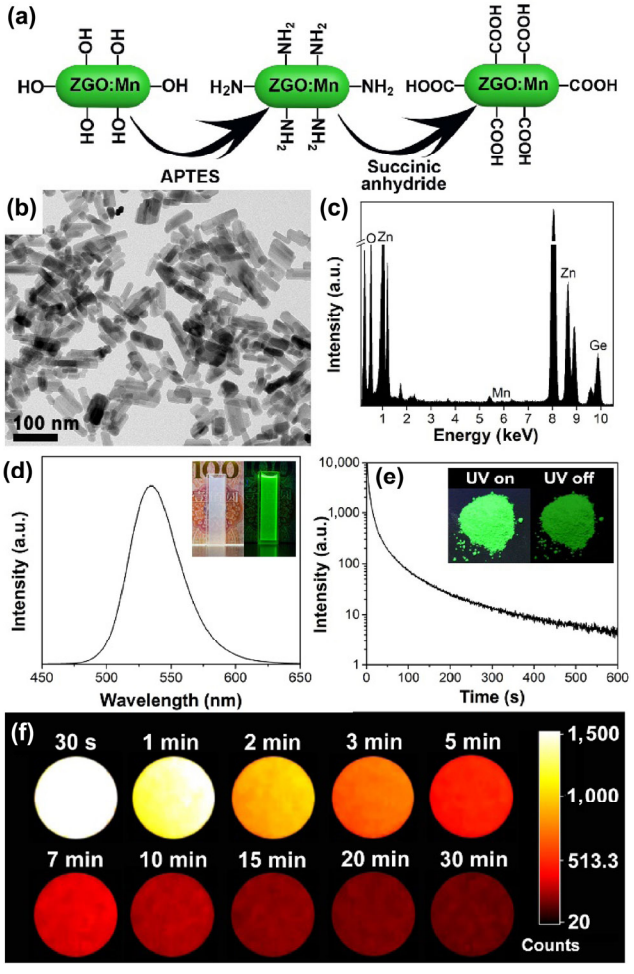

Figure 1 (a) Preparation of the ZGO:Mn-COOH PLNRs. (b) TEM image of the ZGO:Mn-COOH PLNRs. (c) EDX analysis of the ZGO:Mn-COOH PLNRs. (d) Emission spectrum of the ZGO:Mn-COOH PLNRs. Inset: the ZGO:Mn-COOH colloid dispersion in ambient light and under UV excitation. (e) Decay spectrum of the ZGO:Mn-COOH PLNRs. Inset: the luminescence images of ZGO:Mn-COOH under excitation and after excitation ceased. (f) Images of the persistent luminescence decay of ZGO:Mn-COOH PLNRs.

PLNRs displayed an obvious persistent luminescence decay and the emission at 534 nm could still be detected after 10 min of decay (Fig. 1(e)), indicating a long persistence time of the ZGO:Mn-COOH PLNRs. Moreover, the inset in Fig. 1(e) shows that the ZGO:Mn-COOH displayed strong green luminescence after excitation ceased, which made it possible to obtain luminescent LFP images after the excitation ceased. The images of the luminescence decay of ZGO:Mn-COOH were further measured and are presented in Fig. 1(f). The decay time of the persistent luminescence of ZGO:Mn-COOH exceeded 30 min. The above results clearly show that the ZGO:Mn-COOH PLNRs were well-dispersed and displayed strong green persistent luminescence after excitation ceased, suggesting their potential use in background-free LFP imaging.

3.2 The pH optimization for LFP imaging with the ZGO:Mn PLNRs

According to previous studies [40–42], with a certain acidic pH range, the LFP ridges are protonated to carry a positive charge, whereas carboxyl group-functionalized contrast agents still possess a negative charge and can bind to the LFP ridges via electrostatic attraction (Fig. 2(a)). The photographs of a portable spray bottle containing a ZGO:Mn-COOH colloid dispersion with a pH value of 3.5 are presented in Fig. 2(b). The ZGO:Mn-COOH colloid dispersion was milky transparent at a pH of 3.5 in ambient light, suggesting the excellent dispersibility of ZGO:Mn-COOH. Bright green luminescence was observed from the acidic ZGO:Mn-COOH colloid dispersion both under excitation and after the excitation ceased. The zeta potentials of the ZGO:Mn-COOH colloid dispersions with different pH values were further measured. As shown in Fig. S8 in the Electronic Supplementary Material (ESM), the zeta potential of the ZGO:Mn-COOH PLNRs gradually increased with the decrease of pH value from 7 to 3, suggesting that protonation of ZGO:Mn-COOH occurred at acidic pH values. The LFP imaging capability of ZGO:Mn-COOH is closely related to its zeta potential. The optimal pH range for LFP imaging was further investigated. As shown in Fig. 2(c), at pH values of 3 and 3.5, LFP images with good separation between the ridges and furrows were obtained, suggesting the specific binding of ZGO:Mn-COOH PLNRs to LFP ridges via electrostatic attraction [40]. Further increasing the pH value to 4 and above lead to a drastic loss of fingerprint ridge details, which can be ascribed to the weak electrostatic attraction between ZGO:Mn-COOH PLNRs and LFP ridges due to the inefficient protonation of the LFPs at higher pH values [42]. Detailed information on the LFPs obtained at a pH of 3.5, including termination, bifurcation, hook, and whorl, can be easily recognized at high-magnification (Fig. 2(d)). The above results suggest that LFPs can be successfully imaged with the ZGO:Mn PLNRs at pH values around 3.5.

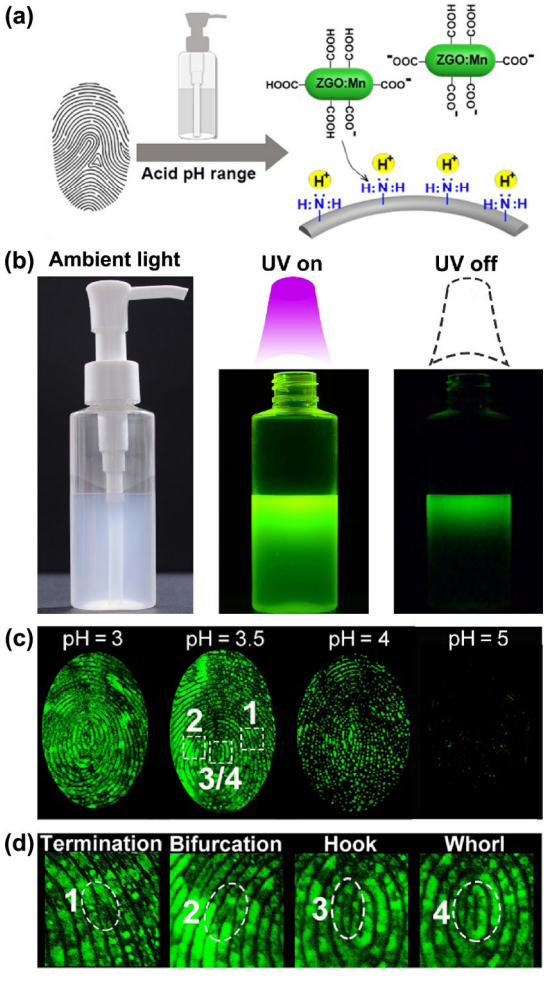

Figure 2 (a) Schematic illustration of pH-mediated imaging of LFPs. (b) Photographs of a spray bottle containing ZGO:Mn-COOH colloid dispersion in ambient light, under UV excitation, and after ceasing UV excitation. (c) Luminescent images of fingerprints treated with ZGO:Mn-COOH PLNR colloid dispersion at different pH values. (d) Specific details of the fingerprint obtained at a pH of 3.5 shown in (c).

3.3 Binding of ZGO:Mn-COOH PLNRs to LFPs

The binding of the ZGO:Mn-COOH PLNRs to the LFP ridges driven by electrostatic attraction under acidic pH was further confirmed by confocal microscopy. The LFPs were stained with a hydrophobic red dye, DiD, and were further treated with the ZGO:Mn-COOH PLNR colloid solution at a pH of 3.5. As shown in Fig. 3(a), the red trace generated by the DiD shows the fingerprint ridges. The green channel shows the distribution of ZGO:Mn-COOH PLNRs on the substrate (Fig. 3(b)). The merged image indicates that the green signal overlaps exactly on the red signal (Fig. 3(c)), which clearly suggests that the ZGO:Mn-COOH PLNRs were bound to the LFP ridges. The three-dimensional (3D) view shown in Figs. 3(d)–3(f) further confirms that the ZGO:Mn-COOH PLNRs specifically bound to the LFP ridges.

3.4 Background-free LFP imaging with ZGO:Mn-COOH PLNRs on problematic substrates

The use of ZGO:Mn-COOH PLNRs in background-free LFP imaging was further tested on daily-encountered problematic substrates like soda cans and cardboard. LFPs were deposited on these two substrates and were further treated with the ZGO:Mn-COOH colloid dispersion. The logo of the soda can showed a red background color in ambient light and also displayed a strong red background fluorescence under UV light (Fig. S9 in the ESM). As shown in Fig. 4(a), under UV excitation, the background fluorescence from the soda can significantly decreased the optical contrast between the LFP ridges and the soda can, leading to poor image resolution and sensitivity. After excitation ceased, the red background fluorescence disappeared completely, whereas the ZGO:Mn-COOH PLNRs still displayed strong green emission due to the long-lived persistent luminescence [43–46]. As a result, a legible fingerprint image with a well-resolved ridge flow was clearly observed. As for the LFP imaging on cardboard with a strong blue background fluorescence (Fig. S9 in the ESM), similar results were observed. Figure 4(b) shows that the fingerprint image was completely hidden by the blue background fluorescence under UV excitation. However, a luminescent fingerprint with clear ridge details was obtained after the excitation

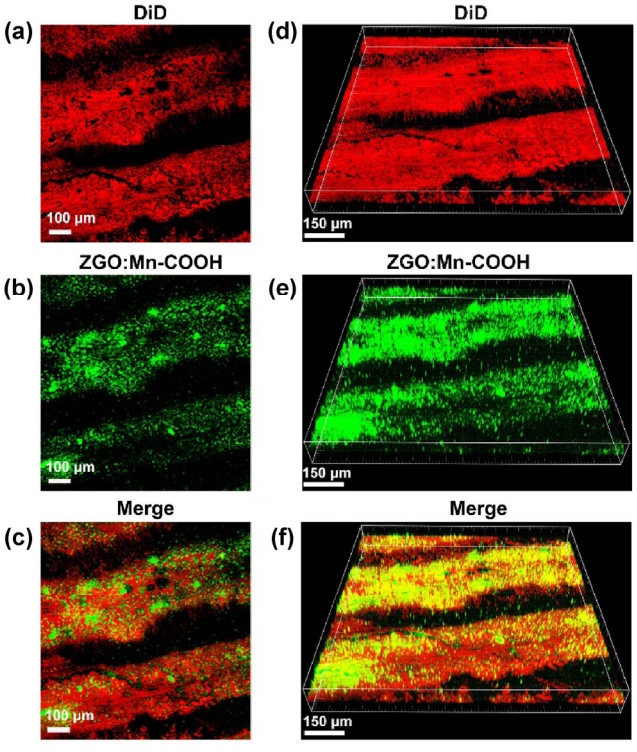

Figure 3 (a)–(c) Confocal microscopy images showing the fingerprint ridge (red channel), ZGO:Mn-COOH PLNRs (green channel), and the merged image. (d)–(f) The corresponding 3D view of the fingerprint ridges.

ceased due to the disappearance of the background fluorescence. The luminescent images in Fig. 4(b) were further transformed into grayscale images (Fig. S10 in the ESM), and the gray value variation across the fingerprints is shown by the yellow line in Fig. 4(c). The gray value showed little change across the fingerprint under UV excitation, and the fingerprint ridges could not be distinguished. In contrast, significant variation of the gray value across the fingerprint was observed after excitation ceased, suggesting a significantly improved optical contrast between fingerprint ridges and the substrate. The above results clearly demonstrated that background interference, such as background color and background fluorescence, could be efficiently eliminated by the ZGO:Mn-COOH PLNRs.

Additionally, we further showed that the ZGO:Mn-COOH PLNRs can be used to eliminate the background interference by an optical filtering method. Since the emission wavelength of the ZGO:Mn-COOH PLNRs is different from that of the cardboard, the blue background fluorescence can also be removed by

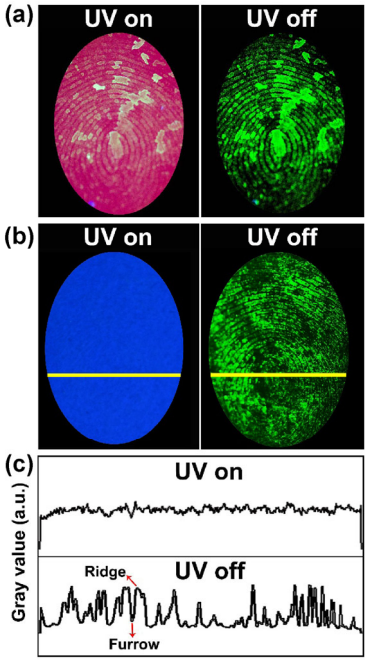

Figure 4 (a) Photographs of a treated fingerprint on the logo of a soda can under excitation (left panel) and after excitation ceased (right panel). (b) Photographs of a treated fingerprint on cardboard under excitation (left panel) and after excitation ceased (right panel). (c) The gray value variation of the fingerprints shown by the yellow line in (b). Transformation of the color images to grayscale images and quantification of the variation of gray value were all conducted with the Quantity One software (Bio-Rad, version 4.6.9).

simply applying a color filter (Fig. 5). The color filter can efficiently block the blue background fluorescence and allow the passage of the green luminescence of the ZGO:Mn-COOH PLNRs to show a clear fingerprint image. These results clearly demonstrated the great flexibility of the ZGO:Mn-COOH PLNRs in eliminating background interference for LFP imaging.

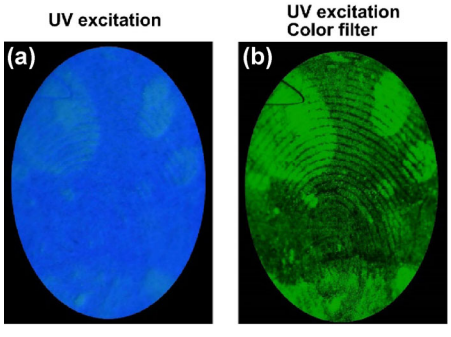

Figure 5 (a) Photograph of a latent fingerprint on a problematic surface under UV excitation without and with (b) a 510 nm long pass filter.

3.5 Investigating the generality of the pH-mediated LFP imaging strategy

As fingerprints encountered in real situations are left on different kinds of substrates, methods for imaging LFPs on surfaces frequently touched in daily life are important for future practical applications. The ability of the pH-mediated LFP imaging method based on the ZGO:Mn-COOH colloid solution with a pH of 3.5 to be used on different surfaces was further tested. Substrates including a mobile phone display screen, a wineglass, scissors, a silicon slice, and wood were examined in this study. As shown in Fig. 6 and Fig. S11 in the ESM, the treated fingerprints on the above-mentioned surfaces all displayed finely-resolved ridge details. It is noteworthy that the uneven surface on the junction of the scissors did not have any obvious destruction to the obtained luminescent fingerprint image (Fig. 6(c)), showing that this LFP imaging strategy can even eliminate the topology interference from the underlying substrates. Thus, the pH-mediated LFP imaging strategy holds great versatility in detecting LFPs deposited on diverse substrates frequently touched in daily life.

Furthermore, the pH-mediated LFP imaging strategy based on ZGO:Mn-COOH PLNRs was used to image the fingerprints from different donors. The luminescent images of the LFPs from different donors after treatment with the ZGO:Mn-COOH PLNR colloid solution at a pH of 3.5 are shown in Fig. 7 and Fig. S12 in the ESM.

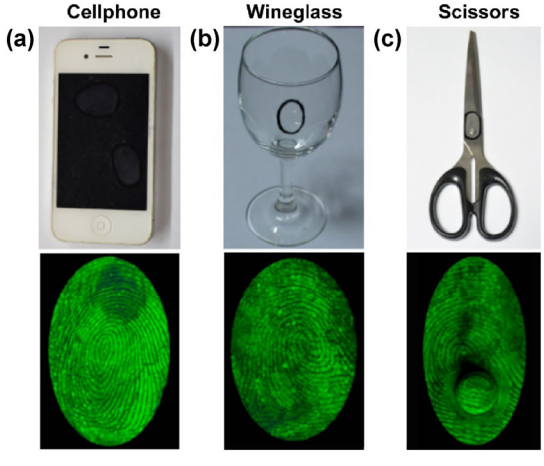

Figure 6 Photographs and luminescent images of treated LFPs on different substrates: (a) a cellphone, (b) a wineglass, and (c) scissors.

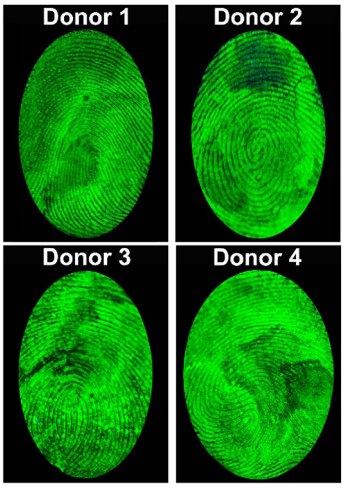

Figure 7 Luminescent images of LFPs from different donors after treatment with the ZGO:Mn-COOH PLNRs.

All the treated LFPs displayed strong green luminescence, showing that this pH-induced imaging strategy can be applied to LFPs from different donors. Moreover, the treated LFPs displayed clear and well-defined papillary ridges without any obvious loss of ridge details. Thus, the above results clearly demonstrated that the pH-mediated LFP imaging strategy based on ZGO:Mn-COOH PLNRs can be applied in various complex situations, suggesting good generality of the developed LFP imaging strategy.

4 Conclusions

In this paper, we have reported a background-free, nondestructive, and easy-to-perform strategy for LFP imaging based on pH-mediated recognition of LFP ridges by ZGO:Mn-COOH PLNRs. ZGO:Mn-COOH can specifically bind to LFP ridges via electrostatic attraction by simply adjusting the pH of the colloid dispersion. Since the ZGO:Mn-COOH can remain luminescent after excitation ceases, background interference such as background color and background fluorescence can be efficiently eliminated by simply capturing the luminescent LFP images after the excitation ceases, leading to a significant improvement of the imaging resolution and sensitivity. Moreover, LFP imaging on different substrates was achieved with the developed pH-mediated imaging strategy, and LFPs from different donors were also successfully detected. To conclude, the developed LFP imaging strategy displays good capability for removing background interference, and it is also nondestructive and easy-to-perform, suggesting its potential for various applications, such as forensic investigation, law enforcement, and anti-counterfeiting authentication.

Acknowledgements

This work was supported by the National Natural Science Foundation of China (No. 21675120), the National Key R&D Program of China (No. 2017YFA0208000), the National Basic Research Program of China (973 Program, No. 2015CB932600), the Open Funding Project of the State Key Laboratory of Biochemical Engineering (No. 4102010299) and the Fundamental Research Funds for the Central Universities (No. 2042017kf0210). Q. Y. thanks the large-scale instrument and equipment sharing foundation of Wuhan University.

Electronic Supplementary Material: Supplementary material (chemicals, instruments, TEM images of ZGO:Mn PLNRs with different surface functionalization, XRD pattern, EPR spectra, zeta potentials, gray scale images of fingerprints, and photographs of fingerprints) is available in the online version of this article at https://doi.org/10.1007/s12274-018-2133-6.

References

[1] Wu, P.; Xu, C. Y.; Hou, X. D.; Xu, J. J.; Chen, H. Y. Dual-emitting quantum dot nanohybrid for imaging of latent fingerprints: Simultaneous identification of individuals and traffic light-type visualization of TNT. *Chem. Sci.* **2015**, *6*, 4445–4450.

[2] He, Y. Y.; Xu, L. R.; Zhu, Y.; Wei, Q. H.; Zhang, M. Q.; Su, B. Immunological multimetal deposition for rapid visualization of sweat fingerprints. *Angew. Chem., Int. Ed.* **2014**, *53*, 12609–12612.

[3] Li, K.; Qin, W. W.; Li, F.; Zhao, X. C.; Jiang, B. W.; Wang, K.; Deng, S. H.; Fan, C. H.; Li, D. Nanoplasmonic imaging of latent fingerprints and identification of cocaine. *Angew. Chem., Int. Ed.* **2013**, *52*, 11542–11545.

[4] Ran, X.; Wang, Z. Z.; Zhang, Z. J.; Pu, F.; Ren, J. S.; Qu, X. G. Nucleic-acid-programmed Ag-nanoclusters as a generic platform for visualization of latent fingerprints and exogenous substances. *Chem. Commun.* **2016**, *52*, 557–560.

[5] Wang, J.; Ma, Q. Q.; Liu, H. Y.; Wang, Y. Q.; Shen, H. J.; Hu, X. X.; Ma, C.; Yuan, Q.; Tan, W. H. Time-gated imaging of latent fingerprints and specific visualization of protein secretions via molecular recognition. *Anal. Chem.* **2017**, *89*, 12764–12770.

[6] Su, B. Recent progress on fingerprint visualization and analysis by imaging ridge residue components. *Anal. Bioanal. Chem.* **2016**, *408*, 2781–2791.

[7] Lee, H. C.; Gaensslen, R. E. *Advances in Fingerprint Technology*, 2nd ed.; CRC Press: Boca Raton, FL, USA, 2001.

[8] Peng, T. H.; Qin, W. W.; Wang, K.; Shi, J. Y.; Fan, C. H.; Li, D. Nanoplasmonic imaging of latent fingerprints with explosive RDX residues. *Anal. Chem.* **2015**, *87*, 9403–9407.

[9] Song, K.; Huang, P.; Yi, C. L.; Ning, B.; Hu, S.; Nie, L. M.; Chen, X. Y.; Nie, Z. H. Photoacoustic and colorimetric visualization of latent fingerprints. *ACS Nano* **2015**, *9*, 12344–12348.

[10] Xu, L. R.; Li, Y.; Wu, S. Z.; Liu, X. H.; Su, B. Imaging latent fingerprints by electrochemiluminescence. *Angew. Chem., Int. Ed.* **2012**, *124*, 8192–8196.

[11] Tang, X. M.; Huang, L. L.; Zhang, W. Y.; Zhong, H. Y. Chemical imaging of latent fingerprints by mass spectrometry based on laser activated electron tunneling. *Anal. Chem.* **2015**, *87*, 2693–2701.

[12] Chen, H. B.; Chang, K. W.; Men, X. J.; Sun, K.; Fang, X. F.; Ma, C.; Zhao, Y. X.; Yin, S. Y.; Qin, W. P.; Wu, C. F. Covalent patterning and rapid visualization of latent fingerprints with photo-cross-linkable semiconductor polymer dots. *ACS Appl. Mater. Interfaces* **2015**, *7*, 14477–14484.

[13] Cui, J. B.; Xu, S. Y.; Guo, C.; Jiang, R.; James, T. D.; Wang, L. Y. Highly efficient photothermal semiconductor nanocomposites for photothermal imaging of latent fingerprints. *Anal. Chem.* **2015**, *87*, 11592–11598.

[14] Hazarika, P.; Jickells, S. M.; Wolff, K.; Russell, D. A. Imaging of latent fingerprints through the detection of drugs and metabolites. *Angew. Chem., Int. Ed.* **2008**, *47*, 10167–10170.

[15] Brunelle, E.; Huynh, C.; Le, A. M.; Halámková, L.; Agudelo, J.; Halámek, J. New horizons for ninhydrin: Colorimetric determination of gender from fingerprints. *Anal. Chem.* **2016**, *88*, 2413–2420.

[16] Xu, C. Y.; Zhou, R. H.; He, W. W.; Wu, L.; Wu, P.; Hou, X. D. Fast imaging of eccrine latent fingerprints with nontoxic Mn-doped ZnS QDs. *Anal. Chem.* **2014**, *86*, 3279–3283.

[17] Chen, X.; Xu, W.; Zhang, L. H.; Bai, X.; Cui, S. B.; Zhou, D. L.; Yin, Z.; Song, H. W.; Kim, D. H. Large upconversion enhancement in the "islands" Au–Ag alloy/$NaYF_4$:Yb^{3+}, Tm^{3+}/Er^{3+} composite films, and fingerprint identification. *Adv. Funct. Mater.* **2015**, *25*, 5462–5471.

[18] Xu, L. R.; Zhang, C. Z.; He, Y. Y.; Su, B. Advances in the development and component recognition of latent fingerprints. *Sci. China Chem.* **2015**, *58*, 1090–1096.

[19] Wang, J.; Wei, T.; Li, X. Y.; Zhang, B. H.; Wang, J. X.; Huang, C.; Yuan, Q. Near-infrared-light-mediated imaging of latent fingerprints based on molecular recognition. *Angew. Chem., Int. Ed.* **2014**, *53*, 1616–1620.

[20] Ramotowski, R. *Lee and Gaensslen's Advances in Fingerprint Technology*, 3rd ed.; CRC press: Boca Raton, FL, USA, 2012.

[21] Menzel, E. R. Recent advances in photoluminescence detection of fingerprints. *Sci. World J.* **2001**, *1*, 498–509.

[22] Frick, A. A.; Busetti, F.; Cross, A.; Lewis, S. W. Aqueous Nile blue: A simple, versatile and safe reagent for the detection of latent fingermarks. *Chem. Commun.* **2014**, *50*, 3341–3343.

[23] Li, Y.; Xu, L. R.; Su, B. Aggregation induced emission for the recognition of latent fingerprints. *Chem. Commun.* **2012**, *48*, 4109–4111.

[24] Li, Z. J.; Zhang, Y. W.; Wu, X.; Huang, L.; Li, D. S.; Fan, W.; Han, G. Direct aqueous-phase synthesis of sub-10 nm "luminous pearls" with enhanced *in vivo* renewable near-infrared persistent luminescence. *J. Am. Chem. Soc.* **2015**, *137*, 5304–5307.

[25] Wang, J.; Ma, Q. Q.; Zheng, W.; Liu, H. Y.; Yin, C. Q.; Wang, F. B.; Chen, X. Y.; Yuan, Q.; Tan, W. H. One-dimensional luminous nanorods featuring tunable persistent luminescence for autofluorescence-free biosensing. *ACS Nano* **2017**, *11*, 8185–8191.

[26] Wu, B. Y.; Wang, H. F.; Chen, J. T.; Yan, X. P. Fluorescence resonance energy transfer inhibition assay for α-fetoprotein excreted during cancer cell growth using functionalized persistent luminescence nanoparticles. *J. Am. Chem. Soc.* **2011**, *133*, 686–688.

[27] Wu, S. Q.; Yang, C. X.; Yan, X. P. A dual-functional persistently luminescent nanocomposite enables engineering of mesenchymal stem cells for homing and gene therapy of glioblastoma. *Adv. Funct. Mater.* **2017**, *27*, 1604992.

[28] le Masne de Chermont, Q.; Chanéac, C.; Seguin, J.; Pellé, F.; Maîtrejean, S.; Jolivet, J. P.; Gourier, D.; Bessodes, M.; Scherman, D. Nanoprobes with near-infrared persistent luminescence for *in vivo* imaging. *Proc. Natl. Acad. Sci. USA* **2007**, *104*, 9266–9271.

[29] Wang, J.; Ma, Q. Q.; Wang, Y. Q.; Shen, H. J.; Yuan, Q. Recent progress in biomedical applications of persistent luminescence nanoparticles. *Nanoscale* **2017**, *9*, 6204–6218.

[30] Liu, H. Y.; Hu, X. X.; Wang, J.; Liu, M.; Wei, W.; Yuan, Q. Direct low-temperature synthesis of ultralong persistent luminescence nanobelts based on a biphasic solution-chemical reaction. *Chin. Chem. Lett.*, in press, DOI: 10.1016/

j.cclet.2018.02.005.

[31] Li, N.; Diao, W.; Han, Y. Y.; Pan, W.; Zhang, T. T.; Tang, B. MnO_2-modified persistent luminescence nanoparticles for detection and imaging of glutathione in living cells and *in vivo*. *Chem.—Eur. J.* **2014**, *20*, 16488–16491.

[32] Chen, L. J.; Yang, C. X.; Yan, X. P. Liposome-coated persistent luminescence nanoparticles as luminescence trackable drug carrier for chemotherapy. *Anal. Chem.* **2017**, *89*, 6936–6939.

[33] Wang, J.; Ma, Q. Q.; Hu, X. X.; Liu, H. Y.; Zheng, W.; Chen, X. Y.; Yuan, Q.; Tan, W. H. Autofluorescence-free targeted tumor imaging based on luminous nanoparticles with composition-dependent size and persistent luminescence. *ACS Nano* **2017**, *11*, 8010–8017.

[34] Abdukayum, A.; Chen, J. T.; Zhao, Q.; Yan, X. P. Functional near infrared-emitting Cr^{3+}/Pr^{3+} Co-doped zinc gallogermanate persistent luminescent nanoparticles with superlong afterglow for *in vivo* targeted bioimaging. *J. Am. Chem. Soc.* **2013**, *135*, 14125–14133.

[35] Abdukayum, A.; Yang, C. X.; Zhao, Q.; Chen, J. T.; Dong, L. X.; Yan, X. P. Gadolinium Complexes functionalized persistent luminescent nanoparticles as a multimodal probe for near-infrared luminescence and magnetic resonance imaging *in vivo*. *Anal. Chem.* **2014**, *86*, 4096–4101.

[36] Li, Z. J.; Huang, L.; Zhang, Y. W.; Zhao, Y.; Yang, H.; Han, G. Near-infrared light activated persistent luminescence nanoparticles via upconversion. *Nano Res.* **2017**, *10*, 1840–1846.

[37] Wang, Y.; Yang, C. X.; Yan, X. P. Hydrothermal and biomineralization synthesis of a dual-modal nanoprobe for targeted near-infrared persistent luminescence and magnetic resonance imaging. *Nanoscale* **2017**, *9*, 9049–9055.

[38] Song, L.; Li, P. P.; Yang, W.; Lin, X. H.; Liang, H.; Chen, X. F.; Liu, G.; Li, J.; Yang, H. H. Low-dose X-ray activation of W(VI)-doped persistent luminescence nanoparticles for deep-tissue photodynamic therapy. *Adv. Funct. Mater.* **2018**, *28*, 1707496.

[39] Zou, R.; Huang, J. J.; Shi, J. P.; Huang, L.; Zhang, X. J.; Wong, K. L.; Zhang, H. W.; Jin, D. Y.; Wang, J.; Su, Q. Silica shell-assisted synthetic route for mono-disperse persistent nanophosphors with enhanced *in vivo* recharged near-infrared persistent luminescence. *Nano Res.* **2017**, *10*, 2070–2082.

[40] Stauffer, E.; Becue, A.; Singh, K. V.; Thampi, K. R.; Champod, C.; Margot, P. Single-metal deposition (SMD) as a latent fingermark enhancement technique: An alternative to multimetal deposition (MMD). *Forensic Sci. Int.* **2007**, *168*, e5–e9.

[41] Choi, M. J.; McDonagh, A. M.; Maynard, P.; Roux, C. Metal-containing nanoparticles and nano-structured particles in fingermark detection. *Forensic Sci. Int.* **2008**, *179*, 87–97.

[42] Moret, S.; Bécue, A.; Champod, C. Functionalised silicon oxide nanoparticles for fingermark detection. *Forensic Sci. Int.* **2016**, *259*, 10–18.

[43] Song, L.; Lin, X. H.; Song, X. R.; Chen, S.; Chen, X. F.; Li, J.; Yang, H. H. Repeatable deep-tissue activation of persistent luminescent nanoparticles by soft X-ray for high sensitivity long-term *in vivo* bioimaging. *Nanoscale* **2017**, *9*, 2718–2722.

[44] Zhou, Z. H.; Zheng, W.; Kong, J. T.; Liu, Y.; Huang, P.; Zhou, S. Y.; Chen, Z.; Shi, J. L.; Chen, X. Y. Rechargeable and LED-activated $ZnGa_2O_4:Cr^{3+}$ near-infrared persistent luminescence nanoprobes for background-free biodetection. *Nanoscale* **2017**, *9*, 6846–6853.

[45] Lin, X. H.; Song, L.; Chen, S.; Chen, X. F.; Wei, J. J.; Li, J. Y.; Huang, G. M.; Yang, H. H. Kiwifruit-like persistent luminescent nanoparticles with high-performance and *in situ* activable near-infrared persistent luminescence for long-term *in vivo* bioimaging. *ACS Appl. Mater. Interfaces* **2017**, *9*, 41181–41187.

[46] Li, N.; Li, Y. H.; Han, Y. Y.; Pan, W.; Zhang, T. T.; Tang, B. A highly selective and instantaneous nanoprobe for detection and imaging of ascorbic acid in living cells and *in vivo*. *Anal. Chem.* **2014**, *86*, 3924–3930.